
Unconventional Systems Integration

E. Williams, Chair
W. Dally
A. Despain
D. Eardley
D. Hammer
P. Horowitz
J. Katz
N. Lewis
J. Sullivan
R. Westervelt

May 1996

JSR-95-120

Approved for Public Release. Distribution Unlimited.

DISTRIBUTION STATEMENT A

Approved for public release
Distribution Unlimited

19960711 127

JASON
The MITRE Corporation
1820 Dolley Madison Boulevard
McLean, Virginia 22102-3481
(703) 883-6997

DTIC QUALITY INSPECTED 1

REPORT DOCUMENTATION PAGE			Form Approved OMB No. 0704-0188
Public reporting burden for this collection of information estimated to average 1 hour per response, including the time for review instructions, searching existing data sources, gathering and maintaining the data needed, and completing and reviewing the collection of information. Send comments regarding this burden estimate or any other aspect of this collection of information, including suggestions for reducing this burden, to Washington Headquarters Services, Directorate for Information Operations and Reports, 1215 Jefferson Davis Highway, Suite 1204, Arlington, VA 22202-4302, and to the Office of Management and Budget, Paperwork Reduction Project (0704-0188), Washington, DC 20503.			
1. AGENCY USE ONLY (Leave blank)	2. REPORT DATE May 1996	3. REPORT TYPE AND DATES COVERED	
4. TITLE AND SUBTITLE UNCONVENTIONAL SYSTEMS INTEGRATION		5. FUNDING NUMBERS 07-95-8534-A4	
6. AUTHOR(S) W. Dally, A. Despain, D. Eardley, D. Hammer, P. Horowitz, J. Katz, N. Lewis, J. Sullivan, E. Williams (Chair), R. Westervelt		8. PERFORMING ORGANIZATION REPORT NUMBER JSR-95-120	
7. PERFORMING ORGANIZATION NAME(S) AND ADDRESS(ES) The MITRE Corporation JASON Program Office, Z561 1820 Dolley Madison Blvd McLean, Virginia 22102		10. SPONSORING/MONITORING AGENCY REPORT NUMBER JSR-95-120	
9. SPONSORING/MONITORING AGENCY NAME(S) AND ADDRESS(ES) ARPA/TIO 3701 North Fairfax Drive, Arlington, Va 22030-1714		11. SUPPLEMENTARY NOTES	
12a. DISTRIBUTION/AVAILABILITY STATEMENT Approved for Public Release -Distribution Unlimited		12b. DISTRIBUTION CODE Limiter Statement A	
13. ABSTRACT (Maximum 200 words) This report examines some potential near term and long term applications of conventional integration in micro-electro mechanical systems (MEMs).			
14. SUBJECT TERMS		15. NUMBER OF PAGES	
		16. PRICE CODE	
17. SECURITY CLASSIFICATION OF REPORT Unclassified	18. SECURITY CLASSIFICATION OF THIS PAGE Unclassified	19. SECURITY CLASSIFICATION OF ABSTRACT Unclassified	20. LIMITATION OF ABSTRACT SAR

Contents

1	INTRODUCTION	1
2	REVIEW OF SUCCESSFUL IMPLEMENTATION	3
2.1	Analog Devices Accelerometer	3
2.2	JPL CMOS Active Pixel Array	5
2.3	Short-Term Applications using Unconventional Integration . .	7
3	DEVELOPMENTS WITH SHORT-TERM INVESTMENT	11
3.1	IC Cooling	12
3.2	Mechanical Actuators	15
3.2.1	Piezo-Electric Ultrasonic Motors	16
3.2.2	Magnetic Actuators	18
3.3	Independently Addressable Sensor Arrays	22
3.3.1	Optical Imaging	22
3.3.2	Ultra Sound Imaging	24
3.3.3	Mechanical Sensor Arrays	24
3.4	High-Performance Accelerometers	26
4	BREAKTHROUGH TECHNOLOGIES	29
4.1	Scanned Probe Lithography	30
4.2	Atomic Lithography	33
A	APPENDIX: SMALL, CHEAP SENSORS (This Appendix is taken from JSR-95-125, "Microsurveillance of the Urban Battlefield")	37
A.1	General Considerations	37
A.2	Strawman Design of an Emplaced Video Sensor	38
B	APPENDIX: LOW-POWER A/D CONVERSION (This Appendix is taken from JSR-95-145, "Ultrasound")	43
B.1	Overview	43
B.2	Block Diagram	43
B.3	Power Calculation	46
B.3.1	Comparator	46
B.3.2	D/A	47
B.3.3	Logic	49

B.3.4 Example	50
B.4 Other Issues	50
B.4.1 Resolution and Linearity	50
B.4.2 Low-Voltage Operation	51
C APPENDIX: AEROSOL GENERATORS	53

1 INTRODUCTION

In initiating this study, we were asked to survey broadly both near-term and long term potential applications of unconventional integration in micro-electromechanical systems (MEMS). We have considered the impact of unconventional integration on short term needs for inexpensive implementation of new technology in military applications, on already-identified needs for new technological capabilities which will however require continuing development to be achieved, and on areas of scientific investigation in MEMS which have the potential for technological breakthrough, but which require long term development. To limit this survey to a tractable size, we consciously excluded from the study applications of Chemical Sensors, which have been discussed in previous JASON studies (JASON Report JSR-93-140), and we have also excluded opto-electronic systems as these were the focus of a study by the Defense Sciences Research Council during the summer of 1995.

We have broken down the results of our study into three sub-sections. In Section 2 of the report, we have considered the possibility of short-term applications in which the cost benefits of integration within commercial CMOS technology are realized. While there are relatively few MEMS applications that have as yet been implemented in this way, it appears that there is a great potential for cost-effective solutions in a wide range of military applications by taking this approach. In the third section of the report, we discuss miscellaneous applications of integrated systems that have clear potential, but would require continuing development at varying levels to be implemented. Several of these are not implementable within CMOS processing, so that integration would require hybrid procedures and thus potentially higher unit

costs that would be justified only by substantial technological need. Finally, in the fourth section of the report, we discuss areas of investigation in which the integration of electronic and mechanical components have a high, long-term potential pay-off. These involve exploiting the special characteristics of MEMS that arise from their small size scale. Some potential applications are easy to visualize, such as single-electron transistors and atomic-scale lithography.

2 REVIEW OF SUCCESSFUL IMPLEMENTATION

Given the prevailing need to reduce the cost of military applications by using commercial off-the shelf technology wherever possible, we have considered two well-documented cases where unconventional integration has resulted in successful and commercially viable products. These are the Analog Devices Accelerometer, and the JPL CMOS active pixel array. By considering the history of the development of these products, and the nature of their capabilities, we have drawn conclusions about what is feasible in terms of short-term low-cost applications and what can be done to increase the range of military applications that can be addressed using commercial capabilities.

2.1 Analog Devices Accelerometer

There is a well-identified market need for single-axis accelerometers to be used as sensors for safety applications in automobiles. While there are of course already several products available to fill this market need, the potential low cost and small size of an integrated micro-sensor made the development of such a unit commercially attractive. In order to realize the benefits of scale, it was necessary in this development to devise a process in which both the mechanical fabrication of the sensor and the fabrication of its integrated control electronics could be accomplished within the steps of an existing micro-electronic fabrication line. Analog Devices undertook a development process with university collaboration, which after an approximate five-year,

twenty-million dollar program, resulted in a successful product marketable at approximately ten dollars per unit. This low cost was realized by the large market volume of such devices and by the implementation of a design that was compatible with a pre-existing process line with only a small number of post-processing steps.

The accelerometer itself consists of a suspended torsion bar of mass 0.1 mg and resonant frequency 22 kHz. The motion of the torsion bar is sensed capacitively by two interdigitated arrays of plates, each with gap spacing 1.3 mm and capacitance 0.1 pF. The design is optimized for the application at hand, thus having excellent ruggedness and reliability, but relatively poor sensitivity and power consumption. Specifically, the measurement range is ± 50 g, the frequency response is dc to 10 kHz, and the shock survival unpowered is greater than 2000g. However the noise level is $0.05\text{g}/\text{Hz}^{(1/2)}$, which makes the device unsuitable for seismometry or navigation, and the power level is 50 mW, which would present a serious limitation in applications requiring remote operation using a battery as a power source.

The noise level of the accelerometer is a result of a non-obvious scaling law of micro-sensors. While capacitive sensing is improved with small electrode gaps, the quality factor Q of a resonator is rapidly degraded with gap size due to viscous damping in air. Specifically, as device size becomes small, the noise due to Brownian motion scales as $\sqrt{4kT\omega/MQ}$, thus requiring large quality factors for good performance. However, squeeze-film damping in air degrades the quality factor by an amount proportional to the ratio of the spacing cubed to the viscosity of the damping medium. Techniques for overcoming this fundamental problem, as well as other problems that arise

in capacitive sensing, are the subject of on-going activity in accelerometer design, as discussed in Section 3 of this report.

2.2 JPL CMOS Active Pixel Array

The very large market for imaging detectors is now dominated by charge-coupled devices (CCD's). The operating principle of the CCD, in which each MOS photo-detector is also used as an element in the readout path via charge transfer, is an accident of the technological capabilities at the time of its development. The obvious technology for information readout would involve using an active transistor coupled to each pixel to allow the charge from the photodetector to be integrated to form an output voltage. However, in the early 1970's when CCD's were developed, the limits of feature size for fabrication of microelectronics was nearly 10 μm . Thus it was necessary to limit strictly the number of electronic elements in order to maintain a reasonable fill factor for the detector. As the lithographic size scale has shrunk to the micron regime, these considerations are no longer so stressing. However, in the intervening twenty years, CCD technology has been developed to a fine art, and there is a large market of products designed specifically around its capabilities and specifications. Thus, even though active pixel technology is likely in the long term to surpass CCD technology in price and possibly also in performance, there is a large activation barrier to be surmounted to accomplish this change.

The benefits of active pixel technology over CCD technology stem in large part from the fact that active pixel detectors can be fabricated using standard CMOS process lines, whereas CCD technology requires specialized,

dedicated process lines. Ultimately, the ability to use CMOS processing promises low price and design flexibility in fabrication of active pixel sensors. The fact that the active pixel sensor is operated totally with CMOS electronics also provides the benefit of low-power operation. In contrast, CCD detectors require a large bias voltage to accomplish efficient charge transfer, and typically require four times as much power to operate as an active pixel array. While at present, the performance of active pixel sensors does not match the optimum performance of scientific CCD's, improvements in output noise are continuing, and for many applications the performance is already adequate. For future applications, one of the most attractive features of the active pixel technology is the on-board processing capability stemming from the independent addressability of the pixels (see Subsection 3.3).

Initially the development of CMOS active pixel imaging arrays at JPL was driven by the need for radiation-hard, low power imagers for space applications. While these motivations remain, the potential applications in other venues such as video network systems provide additional motivation. The technology has been demonstrated for 256×256 arrays implemented in 1.2 micron CMOS with on-board timing and control electronics, for 128×128 arrays optimized for high speed performance up to frame rates of 8 kHz, and for 176×144 arrays with on-board analog-to-digital conversion providing digital output. The latter example provides the most telling demonstration of the improved capabilities in terms of power and size available using this technology. The digital format allows the size of the entire detector to be reduced to approximately a square centimeter, and the power consumption to 35 mW. Interestingly, the use of the on-board ADC (in a column format) actually reduces power consumption, as the use of more efficient digital output amplifiers, rather than analog amplifiers, offsets the power cost of the

ADC. Because the chip can be produced using standard processing lines, the per unit cost of the digital imaging chip is likely to be less than \$50.

2.3 Short-Term Applications using Unconventional Integration

There are many readily identifiable military needs for small, inexpensive, and readily deployable sensors of a variety of sorts. An example of such an application, a deployable video communication unit, is presented in Appendix A. Obviously, wherever possible, the use of commercial technology will provide the most cost-effective solution. However, in cases where commercial technology is not yet available, where there is not sufficient market force to drive development of technology, or where technological superiority is needed, then development of custom technology must be considered. The lessons from the successful implementation of integration discussed above suggest that custom technology can be developed at unit costs that are not exorbitant. The keys to development of affordable custom technology are: 1) design specifications that fulfill, but do not exceed the requirements of the job, 2) use of standardized design tools that are compatible with CMOS fabrication lines, and 3) attention to electronics design with regard to power usage. Each of these three considerations is inter-dependent on the others.

The importance of performance-specific design was illustrated for the Analog Devices accelerometer. The sensor design was restricted to a limited sensitivity, which was sufficient for the specific application, to allow it to be fabricated almost entirely within a standard CMOS process. Over-specification, for instance in either frequency response or sensitivity, could

easily have made this impossible. As we will see in the following section, meeting high-performance specifications is likely to require departures from standard process line conditions. Thus, design specifications for low-cost applications will generally have to encompass compromises to allow an optimization of desired sensor performance and size versus affordability.

The use of standardized design tools compatible with CMOS fabrication lines would have the benefit of reducing unit production costs for a sensor: the set up costs for a fabrication process within an existing line are on the order of one hundred thousand dollars. Thus custom runs of thousands of units become cost effective as long as successful designs can be implemented with a small number of trials. To encourage the development of sensors compatible with low-cost processing, an up-front investment in the implementation and testing of standard designs for sensors and control/amplification units is needed. A prototype for such standardization is the MOSIS consortium which supports research in integrated circuits. Once in place, such standards can serve as the basis for assembling workable, low-cost custom sensors on a mix and match basis governed by performance needs. For this exercise to be fruitful, attention must be paid not only to fabrication process compatibility, but also to preparing serious evaluations of the performance specifications within the standard design tools. This is obviously important to allow designers to match performance levels to their needs, and thus avoid the excess costs of over-design. Performance evaluation is even more important to provide a quantitative recognition of the performance limitations that will be imposed by any standardization scheme that is chosen. The quantification of these limitations should serve as a basis for the selective encouragement of alternative technologies needed for fabrication of future high performance sensors and actuators.

Finally, as illustrated in Appendix A, power use will often be a serious constraint for military applications. Different design choices within existing technologies may optimize power use, with or without performance degradation. For instance, the use of parallel ADC channels on the JPL active pixel sensor allows the use of slower converters, which results in lower power use than a single, faster converter would require. As illustrated in Appendix B, intelligent modification of existing technology, or moderate investment in new technology may also allow substantial improvements in conversion power requirements. Developments in low power amplifiers for MEMS applications are already underway in K. Pister's group at UCLA.

3 DEVELOPMENTS WITH SHORT-TERM INVESTMENT

While we have not attempted to survey the entire field of MEMS, in the course of this study, a number of specific interesting applications of MEMS technology became apparent. All of the applications discussed here require a research investment before useful technology will result, however the potential for useful applications appears high in all cases. The first possibility discussed is the possibility of fabricating a closed-cooling system for integrated circuits based on the principles of heat pipes. We then discuss two types of mechanical actuators with functions that are likely to be important in fabricating small robotic systems. Both of these examples require the use of materials that are not compatible with CMOS process lines and thus face special development problems as compared with the types of devices discussed in Section 2. However, the importance of the potential applications is such that the short term optimization discussed in Section 2 should not be allowed to derail the evolution of alternative technologies such as these. Special opportunities also are likely to result as sensor arrays are developed with independent control electronics, as foreshadowed by the active pixel array. Such arrays may be fabricated either within CMOS-compatible processes or by other means. Their special capabilities will be realized by development of techniques to address individual sensors (pixels) independently to accomplish various sorts of on-board processing. Finally, we present a brief overview of the development of high-performance accelerometers. This is an example where performance is the over-riding concern in a cost/performance analysis,

necessitating development that may not be fully satisfied within conventional CMOS processing constraints. Other applications stemming from MEMS technology are discussed in Appendices C.

3.1 IC Cooling

Heat pipes have been suggested for removing heat from an integrated circuit. Narrow channels may be formed, by a variety of processes, under the circuit to carry cooling fluid. In a narrow channel the capillary forces of the wall are strong, and a wick is not necessary if the dimensionless wick parameter

$$W \equiv \frac{\rho g r L \sin \theta}{S} \ll 1,$$

where ρ is the fluid's density, S is its spreading pressure on the walls ($S = \sigma_{SV} - \sigma_{LV} - \sigma_{SL}$, where the σ 's are surface free energies, and S , L , and V denote solid wall, liquid and vapor, respectively; if $S > 0$ the liquid spreads spontaneously, as assumed here), r is the radius of a cylindrical channel, L is its length and θ is its angle to the horizontal. For a horizontal channel $\theta = 0$. Even for a vertical channel, typical parameters $\rho = 1 \text{ gm/cm}^3$, $r = 0.01 \text{ cm}$, $L = 1 \text{ cm}$ and $S = 100 \text{ erg/cm}^2$ yield $W = 0.1$, justifying the neglect of gravity. If gravity is important, a wick, which reduces the effective value of r by dividing the channel into smaller subchannels between its fibers, is necessary, but we do not consider this here.

The walls of the channel are then coated with a liquid film of thickness d . In steady state the mass flow rate of vapor from hot to cold in the open

channel of radius $r - d$ is

$$Q_v = \frac{\pi}{8} \frac{dp_v}{d\ell} \frac{(r - d)^4}{\nu_v},$$

where $\frac{dp_v}{d\ell} = \frac{\Delta p_v}{L}$ is the gas pressure gradient driving the flow and ν_v is the gas's kinematic viscosity. The return flow of liquid on the walls may be calculated from the equations for the flow of a viscous fluid in an annular cylinder with a free surface on the inside. The result is elementary but cumbersome, and leads to an equation which is solved numerically. Instead, we note that the driving force for the flow of the liquid is only its spreading pressure, which is weak in comparison to vapor pressures under typical heat pipe conditions ($S/r \sim 10^4$ dyne/cm², compared to vapor pressures $p_v \sim 10^6$ dyne/cm² in a heat pipe operating near the normal boiling point of its fluid). We therefore assume the liquid nearly fills the pipe ($r - d \ll r$), which maximizes the liquid flow rate driven by the spreading force. Then the usual result for a filled pipe is a good approximation:

$$Q_l = \frac{\pi}{8} \frac{2S}{Lr} \frac{r^4}{\nu_l},$$

where the effective pressure gradient is obtained from the spreading pressure exerted over a circumference $2\pi r$ and distributed over an area πr^2 along a pipe length L and ν_l is the kinematic viscosity of the liquid. We have ignored the velocity of the liquid in calculating the flow of the gas and the viscous stress of the gas in calculating the flow of the liquid. Equating $Q_v = Q_l \equiv Q$ yields an equation for the ratio $\lambda \equiv 1 - d/r$:

$$\lambda = \left[\frac{2S}{Lr} \frac{\nu_v}{\nu_l} \left(\frac{dp}{d\ell} \right)^{-1} \right]^{1/4}.$$

For most fluids of interest, at an operating pressure of one atmosphere and a temperature drop of a few tens of degrees the gas pressure gradient

$\frac{dp}{dz} \sim \frac{p_v}{L} \sim 10^6$ dyne/cm³ and $\frac{\nu_v}{\nu_l} \sim 0.3$, so that typically $\lambda \approx 0.3$, justifying the approximation that the liquid nearly fills the pipe. This would not be the case at much lower vapor pressure or temperature drop, but is a fairly robust approximation because of the $\frac{1}{4}$ power in the expression for λ . The heat flow is

$$P \approx \frac{\pi S r^3}{4 L \nu_l} \Delta H,$$

where ΔH is the enthalpy of evaporation; for most volatile liquids $\Delta H \sim 4 \times 10^9$ erg/gm. Using the previously quoted parameters and $\nu_l = 0.01$ cm²/sec we find that a single pipe carries a power $P \approx 3$ W. A layer of pipes spaced at intervals of 500 μ (20/cm) can carry 60 W away from a 1 cm square chip. Because of the nonlinearity of the heat pipe, its heat flow is only a weak function of the temperature gradient unless this is so slight, or the vapor pressure is so small, that $\frac{dp_v}{dz}$ is insufficient to drive enough vapor (and its latent heat) to carry the assumed heat flux. Heat pipes appear to be promising means of cooling high power dissipation microelectronic chips, but it must be remembered that ideal performance has been assumed, and a number of approximations have been made. Real performance may not be as good. The calculated power is also a sensitive function of pipe diameter; 100 μ diameter pipes (half that assumed here) would carry only $\frac{1}{8}$ as much heat each, or $\frac{1}{4}$ as much in a filled layer. We have not specified the working fluid, except to assume that it wets the silicon with a spreading pressure of 100 dyne/cm².

The quantity of fluid in the pipe must be carefully chosen: at the operating temperature the hot end must evaporate almost dry, in order that the full spreading pressure be available to drive the flow of liquid, but the meniscus must extend up to this region of evaporation in order that a flow of liquid be available there. To achieve this, after the pipe fills with vapor

at the equilibrium vapor pressure at the temperature of the hot end, some liquid must be left over to wet the walls. The temperature of the hot end may adjust to maintain this condition.

A wick has the effect of decreasing the radii of the fluid-carrying channels. Because the flow per channel is proportional to r^{-3} and the number of channels can increase no faster than r^2 , a wick reduces the heat carrying capacity of a heat pipe unless it is required because capillarity is insufficient to transport the liquid. This is the case if the liquid does not wet the walls of the pipe or if gravity is important (W is not small).

The theory of heat pipes is well developed, and is discussed in many publications (*cf. Heat Pipes*, P. D. Dunn and D. A. Reay, Pergamon Press, 3rd ed. 1982).

3.2 Mechanical Actuators

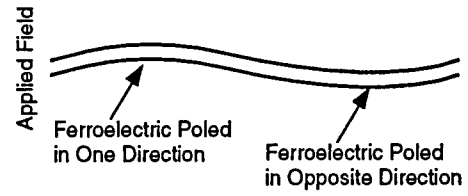
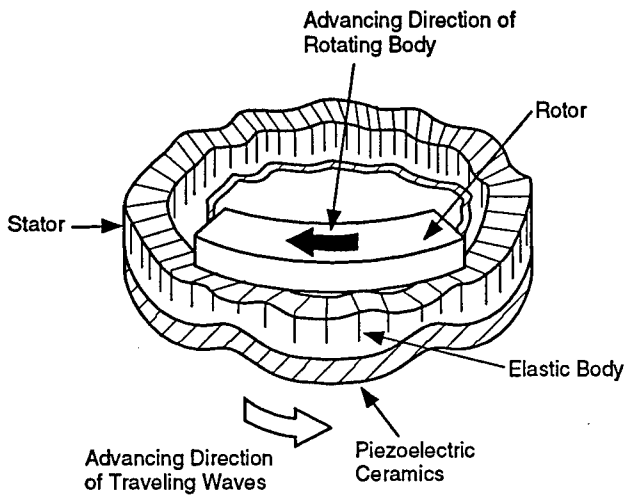
Micro-sensors are generally better suited to implementation within a purely Si-based process than are micro-actuators. Exceptions to this are actuators to be used as light deflectors, which require little mechanical strength. In addition, some progress has been made in developing fluid switches within a Si technology. However, these are generally slow and bulky. In applications requiring speed or the application of large forces, actuators made of other materials generally perform better. Since alternative materials are anathema to CMOS process lines, such actuators are not candidates for direct integration. However, since actuators are often larger than sensors, and often are part of more expensive systems, the benefits of integration in any case may

not be as overwhelming for actuators as for sensors. Thus while short-term benefits will obviously focus investment in CMOS-compatible technology, the development of alternative materials technologies should not be neglected as a result.

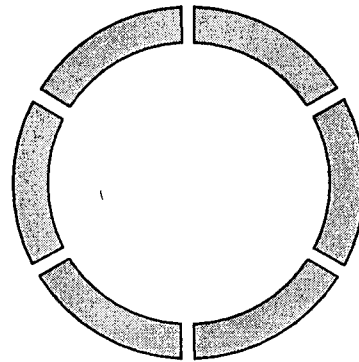
We review here two interesting actuator technologies with potential importance in developing small mobile robots. The first, piezo-electric motors, is still in the development stage and requires continuing work. The second, magnetically actuated flaps, is a working technology which we present in context of a potential application in developing small fliers.

3.2.1 Piezo-Electric Ultrasonic Motors

Piezo-electric ultrasonic motors represent a novel motor design in which vibrational motion is transformed into rotational motion via a frictional coupling. The basic principle of an ultrasonic motor is illustrated in Figure 3-1. The source of the vibrations in the motor is a piezo-electric cylinder to which segmented electrodes have been attached. By applying voltages of alternating signs to the electrodes, a standing wave is induced in the cylinder. The piezo-electric cylinder is tightly attached to an elastic material which amplifies the displacements due to the standing wave. The rotor of the piezo-electric motor is placed in frictional contact with the elastic material, and obtains a direct rotational motion as a result of the interaction with the standing wave. Such motors have been developed and commercialized in Japan, and are used for automatic focusing in camera lenses.



(a) Illustration of Distortion of Biomorphic Strip With Field on Poled Ferroelectric Material



(b) Normal Mode Excited on a Ring

Figure 3-1. Piezo-electric ultrasonic motors.

The miniaturization of piezoelectric motors is complicated by the difficulty of working with ceramic piezoelectrics. The possibility of circumventing these difficulties has arisen due to recent materials development in the fabrication of thin film piezoelectric materials using sol-gel processing techniques. This technology appears especially attractive as a method of incorporating piezo ceramics directly onto a silicon substrate. Using these techniques, A. Flynn at MIT, in collaboration with K.R. Udayakumar of Penn State, has fabricated thin film motors as small as $0.3 \mu\text{m}$ thick and 0.8 mm in diameter and demonstrated the capability to rotate supported lenses at 100-300 rpm, with an estimated torque of 41 pNm. (In contrast, Flynn has demonstrated for a small (8 mm) bulk motor efficient operation with stall torque of approximately 1 mNm.) The results on these thin film motors are a feasibility demonstration only, which indicate the potential of micromotor development in the context of a number of fabrication problems which must be solved to make a workable device. Continuing work on fabricating films that are free of pinholes and in developing processing techniques such as laser etching to form the stator appears promising.

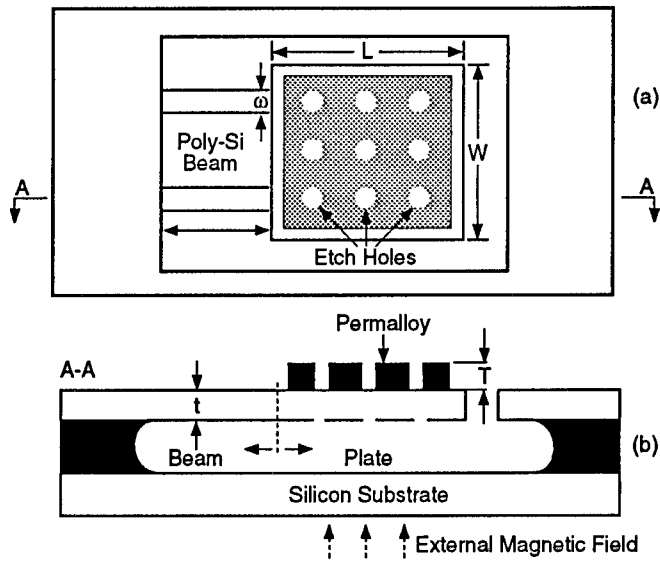
3.2.2 Magnetic Actuators

Small remotely piloted vehicles have numerous battlefield applications, chiefly in reconnaissance and sensor delivery. We discussed some of these vehicles in JSR 93-150 "Fly on the Wall", and were therefore pleased to learn of Marvin Pope's work at Lincoln Laboratories on "Little Things", airplanes small enough to fit in a hand. One of the problems of such very small airplanes is their control systems. There is concern that it will be difficult to miniaturize conventional model airplane actuators and control surfaces to

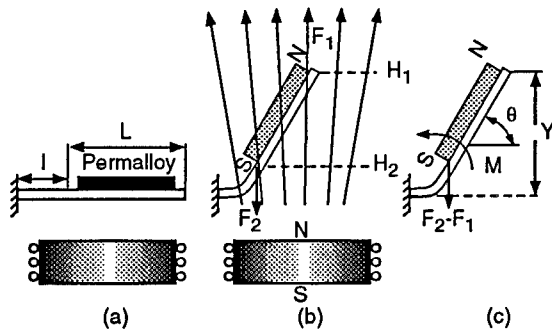
the required sizes. We have not investigated this, but instead describe an application of MEMS technology which may provide an alternative solution.

Y. C. Tai of Cal Tech described for us magnetic actuators developed by his group and collaborators at UCLA. These consist of a permalloy plate electrodeposited on a polysilicon or Si_3N_4 flap, as shown in Figure 3-2 (Liu, *et al.* 1995 Proc. IEEE Micro Electro Mechanical Systems 95CH35754). The plate is perforated to increase the rate of circulation of etching fluid which releases it from its silicon substrate. Underneath the substrate is an ordinary (but small) wire-wound electromagnet. When this electromagnet is energized the permalloy is magnetized to saturation. Once saturated, its magnetic moment is essentially fixed. This strong nonlinearity explains the counter-intuitive behavior illustrated; the saturated permalloy acts nearly as a permanent magnet (a linearly permeable flap would be attracted to the electromagnet, as we see with toy magnets and everyday ferromagnetic materials of moderate permeability). The flap is 1 mm on a side, and can be bent to a deflection angle of 70° by the coil.

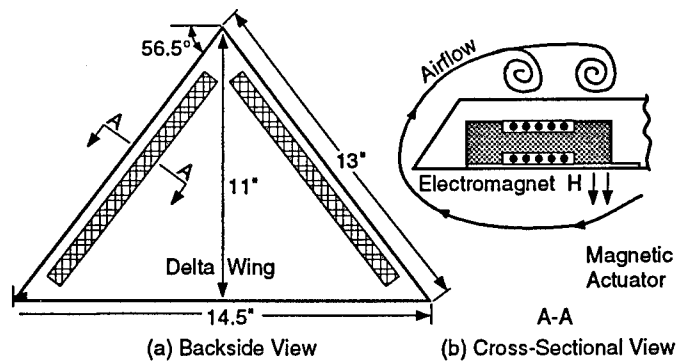
The deployment of such a flap mounted on an airfoil will change the airflow and hence the lift and drag. Liu, *et al.* mounted a linear array of such flaps near the leading edge of a model delta wing with a span of 37 cm. Under certain flight conditions, deploying the flap on one side of the delta wing in a low speed wind tunnel (air speed 16 m/sec) was observed to produce rolling moments corresponding to a lift asymmetry of roughly 1%. Use of a fixed flap of similar dimensions, but mounted on the leading edge of the wing, produced lift asymmetries of as much as 10%. This is more than adequate to control an airplane, and even larger lift asymmetries should be



Schematic of an out-of-plane permalloy magnetic actuator (a micro-flap).



Magnetic actuation of a flap by an external electromagnet. (a) Rest position when $H_{ext}=0$; (b) out-of-plane actuation when $H_{ext}\neq 0$; (c) out-of-plane actuation when $H_{ext}=0$; F_1 and F_2 are the induced magnetic forces on the upper and lower edges of the plate; (c) a simplified analytical model of the flap; the effective bending moment, M is $F_1 L \cos\theta$.



Schematic of a delta-wing with two linear arrays of magnetic actuators flush-mounted close to the leading edges. (a) Plane view of a delta-wing with actuators installed; (b) cross-sectional view of the actuator/electromagnet on the delta-wing.

possible on smaller wings, for which the flap is proportionally larger. The speed of 16m/sec is realistic for a small flier.

The limitations of this result must not be forgotten. An asymmetry of 10% is obtained only for a flap at the leading edge. The actual actuator used in these experiments is not strong enough to deploy the flap against aerodynamic forces in this position, so that this result could only be obtained for a fixed (non-actuated) flap. For actuated flaps at the position shown in Figure 3-2 the asymmetry never exceeded 1.2%, but stronger actuators should make the greater figure (10%) possible. The most important limitation of these results is that they were obtained at an angle of attack of 30°. This is unrealistic for steady flight, and may be close to the stall condition. At stall threshold the lift would be expected to be sensitive to small changes in airfoil configuration, and it is therefore not surprising that the motion of small flaps could produce large changes in lift.

Despite the limited usefulness of the extant results, magnetic micro-machined mechanisms may prove to be useful actuators for flight control of small fliers. With wing spans of ~ 10 cm, control surfaces must have ranges of motion of 1–10 mm. Achieving this with piezoelectrics would require inverse levers of extremely small mechanical advantage, which are probably impractical. Magnetic actuators do not suffer from this limitation, and exert much larger forces than electrostatic actuators.

The preliminary aerodynamic results should therefore be regarded as encouraging, however limited and unrealistic their flight regime. However, there is no aerodynamic “magic” which would permit a 1 mm flap to provide useful torque for a full-sized airplane. Such a flap can change the position at which a vortex forms or a flow separates, but only by a distance of order

its own size. Hence the lift asymmetry can only be of order the ratio of flap size to wing chord, times a factor nominally of order unity but possibly an order of magnitude larger under favorable (carefully chosen) conditions, as in these experiments.

3.3 Independently Addressable Sensor Arrays

The Active Pixel Sensor, discussed in Subsection 2.2, can be considered as the prototype for a new possibility that arises due to the shrinking size of MEMS, that is the fabrication of arrays of independently addressable sensors. Under conditions where a sensor is in a remote location, and communication of output is stringently limited by power use, on-board processing and data compression may become the keys to a usefully functional sensor.

3.3.1 Optical Imaging

In an imaging array of optical sensors, the possibility of independent and parallel access to each pixel offers many new advantages. For example, each pixel sensor can have its own “nano-processor” that communicates to its nearest neighbors and a global command processor. The global processor issues commands (in parallel) to each nanoprocessor. [This is similar to a connection machine] The result is a specialized single instruction, multiple data (SIMD) computer with a pixel sensor directly wired to each computing element, detecting and processing images under program control, all on a single chip. The nano-processors are extremely simple ‘one-bit’ processors with a simple comparator connected to the optical sensor, so that analog to

digital conversion is accomplished in software.

Because all image detection, conversion and processing steps are accomplished under program control, extremely flexible and powerful image processing can be all accomplished on the sensor chip. Only the final desired result needs to be transmitted off-chip. Thus besides the great reduction in power consumption, size and weight over conventional systems, this approach can greatly reduce the communication bandwidth needed to transmit the information from the sensor.

A number of possible applications come to mind for such an 'intelligent camera':

1. Images sometimes contain very bright objects such as the sun or flares, when there are dim objects of interest in shadows, etc. (Remember what happened to the Red Baron when he did not see his enemy attacking him 'out of the sun'.) Shutting down a single iris to compensate for the bright object, then causes the dim object to disappear. A software program in our intelligent camera can discriminate and block selectively, so that dim objects can be sensed and processed.
2. Often a camera will be set up to monitor a scene to detect some interesting activity. Our intelligent camera can be programmed for example to provide only images of objects that move relative to the scene background.
3. When communication is expensive, the intelligent camera can compress the image according to the task of the camera and the activity in the scene. For some tasks, the output might be only a bit, transmitted when some object of interest is recognized by the intelligent camera.

4. The intelligent camera can also be programmed for image analysis, for example to monitor environmental variables of interest. For example it could report percent cloud cover.
5. The intelligent camera can also be programmed to provide autofocus, camera positioning, zoom, external lighting and other robot operator commands.

In summary, the intelligent camera can provide, powerful and flexible image sensing, image processing, and data compression with large savings in power consumption, weight, size and communication bandwidth.

3.3.2 Ultra Sound Imaging

A similar concept is likely to prove useful in ultrasound detectors as discussed in JASON report JSR-95-145. There, even though pixel sizes are larger, the possibility of handling the output of each pixel independently at the sensor will allow significant advances in the number of pixels that can be used in medical imagery, and in the types of imaging, such as confocal imaging and holography, that may be performed.

3.3.3 Mechanical Sensor Arrays

Independent addressability provides the potential for similar advanced capabilities for arrays of mechanical sensors. One interesting example of such an array is the recent fabrication of an artificial cochlea by N. MacDonald's

group at Cornell. Using special processing techniques (not CMOS standard) which involve fabrication in single-crystal Silicon, they can fabricate vertical resonant bars which can be assembled into closely spaced arrays. To simulate human hearing, they fabricated an array of beams of lengths ranging from 400 to 7000 μm , tailored to give a resonant frequency that varied exponentially along the array. To mimic the effect of the critical bands of frequency response in hearing, different arrays were fabricated with gaps varying from 4 μm to 20 μm to vary the coupling between the beams which arises from the viscous medium (air) between them. In the first implementation, the response of the beams was individually monitored via the Doppler shift of a reflected laser beam. The development of on-board electronic monitoring is underway via the incorporation of piezoelectric elements at the ends of the resonators. The same group has also pioneered the incorporation of a FET into the fabrication process. In the future, this should allow front-end electronics to be incorporated directly into the mechanical elements. Such a capability opens the possibility of independently addressable arrays of mechanical sensors with on board processing capabilities analogous to those discussed for the active pixel array.

Similar resonator arrays, but at even higher frequencies, up to the GigaHertz range, are a likely outcome of the work of M. Roukes at Caltech. Extremely small single resonators have been fabricated in single crystal silicon, using a variant of the process developed at Cornell. They achieve (in vacuum) extremely high quality factors as well as high frequencies. The incorporation of piezo-electric elements allows either frequency tuning or individual sensing. Extension of these structures to arrays opens the possibility of fabrication of single-chip high frequency spectrometers and filters.

3.4 High-Performance Accelerometers

The demands of high-performance in certain sensing applications such as navigation and surveillance present serious challenges in devising micro-sensors. Here we discuss just one type of sensor, an accelerometer, and note three different approaches to MEMS implementation of a device with extremely high sensitivity. The theory of accelerometer design is well known: an accelerometer consists of a proof mass suspended by a spring from an external mounting, and a detection system to measure the displacement of the mass in response to acceleration of the external mounting. In the case where the frequency of the acceleration to be measured is substantially less than the resonant frequency of the spring/mass system, the accelerometer response (the displacement) to the input acceleration a in the frequency domain is simply $Z_S(f) = a/\omega_o^2$, where the resonant frequency $\omega_o = \sqrt{k/m}$ and the input acceleration is in meters per second squared per root Hertz. The signal-to-noise ratio at any frequency is $\sqrt{\frac{mQ}{4K_B T \omega_o}}$ which can become very poor when the mass is small enough that Brownian motion is significant. Design of a high-performance instrument requires an extremely sensitive method of measuring the displacement, as well as optimizing the fundamental limits of the signal to noise. Several different approaches to the design of high-performance accelerometers are underway.

The use of capacitive sensing of the gap spacing of the accelerometer is being pursued by W. Kaiser of UCLA. In addition to the problem of viscous damping (see Subsection 2.1) which drives down the quality factor of the spring system, and thus increases the noise, stray capacitances and reference voltage stability also present serious practical problems in achieving

high performance. Kaser's group is addressing these problems by using bulk micromachining steps to improve the mechanical performance, a suspended measurement electrode to reduce parasitic capacitance, and a balanced capacitance bridge measurement with the feedback to reduce problems of reference stability. The bulk micro-machining requires a CMOS post-processing step. Not all of these improvements have yet been incorporated in an optimized accelerometer design. However, the first accelerometer designed using this approach and a large proof mass (10 g) achieved a noise level of $10^{-9}g/Hz^{1/2}$, which is within the limits needed for a navigational accelerometer.

Another approach to position sensing is being explored by the group of T. Kenny at Stanford. Here, the decreasing size of the accelerometer is exploited to advantage by using electron tunneling as a displacement sensing mechanism. Because the tunneling current varies exponentially as the separation, this approach has the immediate benefit of extremely high sensitivity. However, $1/f$ noise is a problem in tunneling, so that this technique encounters noise limitations at low frequencies. Its first applications may therefore occur in surveillance rather than in navigation. Early tests of accelerometers based on this principle have yielded displacement response of 10^{-4} to 10^{-5} Å/ $Hz^{1/2}$ and noise levels of $2 \times 10^{-7}g/Hz^{1/2}$. This result was achieved under relatively unfavorable conditions of a small proof mass (3 mg) and a low Q suspension, suggesting that large improvements in performance are possible.

Finally, another highly sensitive displacement sensor has been developed by the group of M. Roukes at Caltech. They have fabricated extremely small vertical resonant beams with resonant frequency up to gigahertz. They are able to sense displacements of these beams by applying externally a large

magnetic field and then monitoring the ac response of a current through a closed circuit including the beam as part of the circuit path. Displacements of the beam alter the area of the closed circuit, and in turn the inductive response. In this way they are able to sense beam displacements with sensitivity as small as $10^{-4} \text{ \AA/Hz}^{1/2}$, comparable to the sensitivity of a tunnel sensor. Development of this technique for seismometry seems feasible.

The approaches being used to develop high performance accelerometers will also be applicable to a wide variety of other types of sensors. Other proposed applications include infrared detection, magnetometry, audio and ultrasound detection.

4 BREAKTHROUGH TECHNOLOGIES

As the techniques of microfabrication are continually being improved and pushed to smaller length scales, it becomes possible to address problems of fundamental interest and potential application that were not earlier possible. Extremely interesting work on the properties of ultra-small structures is being performed by the group of Roukes at Caltech. By fabricating single crystalline structures of submicron length scale, they are able to address a variety of fundamental problems. One problem is the effects on thermal conductance when the phonon wavelength is comparable to the size of the structure. Continuing fundamental work on such problems is likely to lead to new technologies, such as long range potential applications in areas such as radiation detectors and IR imaging arrays. Another problem addressable with extremely small mechanical structures is the observation of quantum mechanical behavior such as zero-point fluctuations. Long-term potential applications stemming from this research include the possibility of fabricating a room-temperature single-electron transistor, which could effect a single charge transfer by deflecting a small cantilever toward a counter-electrode.

Another area of potential applications, where many of the fundamental issues have already been explored, is that of atom-by-atom lithography using scanned probe manipulation or atom focusing. The potential of scanned probe read/write devices capable of achieving information storage densities limited by the size of the atom has been recognized almost since the first invention of STM. However, the practical limitation of the rate at which such data storage might be possible has always been a stumbling block. Recent advances in micro-motion and tip fabrication now offer at least the possibil-

ity that this difficulty could be overcome. An alternative technology which has the advantage of being inherently parallel, is atomic lithography. Both of these potential technologies have passed the stage of early feasibility demonstrations and need focused effort to determine whether, in fact, practical technologies can be developed from them.

4.1 Scanned Probe Lithography

The two problems in scanned probe lithography are the development of appropriate techniques for writing information, and addressing the problem of doing such writing at useful rates. The possibility of writing has been the subject of a wide range of studies with a large number of mechanisms identified. The mechanisms most likely to result in a successful application are those in which a resist is used in a manner analogous to electron beam lithography. Standard e-beam resists have been evaluated for exposure using field emitted electrons from a STM tip, indicating that the lower energy electrons used with the STM tip resulted in improved resolution due to reduced electron scattering. Optimization of resists for STM or AFM exposure is one major effort that will need to be undertaken to develop scanned probe lithography. Two examples of resists that appear highly successful at exposure levels achievable with existing scanned probe techniques are the use of hydrogenated amorphous silicon, and the use of spin-on-glass. In the former case, an amorphous silicon layer is passivated with hydrogen, and then the hydrogen is field-desorbed by passing an AFM tip, with an applied voltage ranging from 4 to 25 V, over the surface. Simultaneous exposure to oxygen causes the de-passivated region to become oxidized and resistant to subsequent chemical or plasma etching. The oxide line widths drawn in this way

are as small as 2 nm wide, depending on the applied voltage and the speed of the scan. Scan speeds on the order of $1\mu\text{m/s}$ are used. The technique has been used by two groups (at NRL and at Stanford) to fabricate FET structures with critical sizes ranging from 30 nm to $0.1\mu\text{m}$. Another resist that has been demonstrated is spin-on-glass (siloxane), which can be deposited and exposed with an AFM tip biased to 70 V and tip-sample currents of a nA. It is believed that the exposure of the resist causes local decomposition with the release of methyl groups forming regions with high organic content that are resist to subsequent oxide etch. Write speeds greater than 1mm/s were demonstrated, with the ultimate rate limited by the response of the scanner rather than the response of the resist.

Quantitative studies of resist sensitivity in both STM and AFM exposure mode will be needed to develop proximal probe lithography. In STM mode, the typical tunneling current is a nano-amp. Once a sensitivity is measured for a tunnel resist, it will be straightforward to apply the same statistical analysis used in e-beam and im-beam lithography to determine the maximum rate for a desired resolution. The same analysis for the AFM mode, however, presents an interesting problem. The exposure mechanism depends on the strength of the electric field rather than a (statistically variable) number of exposing particles. Determining exposure reliability in this case will require some research to improve understanding of the exposure mechanism.

While the development of appropriate resist technology will provide one limit to achievable speeds of scanned probe lithography, another limit will be the speed with which the probe tip can be scanned across the surface. To improve scan speeds, one can devise very rigid, high speed scanners, and one can

consider the use of multiple tips with integrated control electronics. Both of these approaches appear feasible with fabrication techniques that are under development, for instance in N. McDonald's group. The use of single crystal, high-resonance-frequency beams in displacement actuators allows the formation of high frequency (albeit small area) scanning drives. A demonstration of a prototype micro-STM developed at Cornell shows that this approach can be considered seriously. Drive actuators with resonance frequencies above a megahertz have been demonstrated, suggesting a mechanical limitation on write-rates of up to 10^5 lines/s. So far scan areas are limited to a width of a micron or less. To write to this area at 10 nm resolution would only require 1 ms, if only mechanical effects limited the rate. Given that both the speed up control electronics and resist sensitivity will also play a role in determining the rate, this speed, which still corresponds to 10^5 s per square centimeter, would need to be improved for large volume applications. The incorporation of multiple tips onto a scanner, or the use of multiple scanners each with a single tip provide the most obvious methods of increasing write speeds and areal coverage. There are serious engineering problems that would need to be overcome to accomplish this. First, the tips would have to be independently addressable both in terms of applied voltages to control the write pattern, and in terms of height adjustment. Secondly, the relatively small area over which the tip can be scanned compared to the area occupied by the drive mechanism would require either precise stepping of the sample relative to the scanner, or serious modification of the actuator design, or both. The first problem harks back to issues of independently addressable sensor arrays, discussed in Section 2, and clearly can be addressed with developing technology to incorporate electronics onto micro-mechanical structures. The second problem is certainly addressable by extension of existing technology. Rotating a sample under an AFM tip has been demonstrated as a write

mechanism at data rates of 100 kHz, and application of multiple AFM tips has also been demonstrated, although without independent feedback on the individual probes.

Whether all of these issues can be solved to result in a technology competitive or superior to electron or ion beam techniques as design scales shrink into the 0.1 μm regime and below is open to question. However, the fundamental understanding and demonstrations that are in place indicate that there is at least a feasibility of a useful scanned probe lithographic technology. A focused investment into the development of such a technology seems warranted. In addition to potential high-payoff in micro-electronics at shrinking size scales, the technological development of independently addressable tip arrays is likely to have impact in the area of flat panel displays, and in the development of highly focused electron sources.

4.2 Atomic Lithography

By now, laser cooling, and even trapping, of matter is a well known phenomenon. In the context of this study, there is already a possible application: high resolution lithography using cooled beams of atoms. There are several versions of this possibility. In the simplest one, fine lines of metals can be deposited on a wafer as follows: An electron beam is used to create a high resolution mask. The mask is then placed upon (or very close to) the surface of a wafer. A neutral beam of Al or other metal from a thermal source then floods the mask/wafer, depositing conductor where there is no mask. If there were no gap between the mask and the surface, the transverse energy spread of the neutrals would not matter, i.e. there would be no need

to have a highly collimated atomic beam. However, as the wafer begins to develop surface features of, for example, 1 micron in height, the transverse velocity must be below 1/30 of the longitudinal velocity, if, for example 30 nanometer features are to be produced, requiring the neutral beam to have 0.1% or less of its energy in the transverse direction. Gaps larger than 1 micron require even less transverse energy. This can be accomplished with low energy neutral beams by laser-cooling the transverse beam motion. Fifty nanometer feature sizes have been demonstrated with this technique using a Na beam and a 50 mW dye laser (100 micron diameter). The neutrals can do virtually no damage to the surface since they have less than 0.1 eV longitudinal energy.

A more complicated possibility involves neutral He or Ar atoms in a metastable excited state that are generated in a discharge. Because a laser can be used to pump the neutrals out of the metastable state so that they can undergo a transition to the ground state, the laser can bring about the patterning of the neutral beam by its spatial intensity pattern. When the resulting partly still excited and partly quenched neutral beam reaches a specially prepared surface, the regions of the surface exposed to the portion of the beam not de-excited by the laser is damaged and removed by the residual excited state energy. Therefore, with enough neutral beam fluence, the layers(s) underneath the original surface layer can be uncovered and then chemically etched, while the remainder of the underlying layer remains protected.

Since neutral beams from thermal sources are not very intense, it takes minutes to deliver the fluence necessary to carry out a single production step such as depositing interconnects (deposition of 100 Å of Na takes 10

minutes). Therefore, it would seem most interesting to use laser-beam-cooled neutral beams for special purpose lithography that is difficult to do by other means. One such possibility is to cool and focus a uniform neutral beam by the coherent electric field pattern in two crossed laser beams tuned so as to enable stark shift focusing of the neutrals in the beam. A two-dimensional array of focal points in a highly accurate periodic pattern of nanometer-scale fiducial points can be produced at the focal plane. In two dimensions, one-half wavelength spacing has been achieved, and by clever use of a pair of polarized lasers, a one-eighth wavelength pattern of spots has been obtained in one dimension. The focal length can be as short as tens of microns. In order to achieve a one micron depth of field, however, a longer focal length and a longitudinally (as well as transversely) cooled neutral beam would be required.

Beyond this, the question arises as to whether aperiodic patterns can be written on a resist (or equivalent surface layer) by laser-focusing of neutral beams. The idea of using holographic lenses with crossed lasers to produce arbitrary patterns in space to achieve this goal may be possible in principle. However, this possibility is still being investigated theoretically, and its limitations (on resolution, requirements on the gratings, etc.) are not yet worked out.

A APPENDIX: SMALL, CHEAP SENSORS (This Appendix is taken from JSR-95-125, “Microsurveillance of the Urban Battlefield”)

A.1 General Considerations

Now that we have discussed data transport issues, it is time to discuss the sensors that generate the data. We will focus on imaging sensors, not because other types are uninteresting, but because the video sensor poses the hardest design problem and generates the bulk of the data.

We need a miniaturised, low-power combined sensor and communications package cheap enough to be treated as a throwaway item. The familiar CCD detector technology appears to be incompatible with the requirements of our problem for reasons of both cost and power consumption. However, a new detector technology, called CMOS active pixel arrays, appears ideally suited to our needs. The important facts about it are that: the pixel array is created by standard CMOS manufacturing steps and can be integrated on a single chip with processor and memory; individual pixels can be directly addressed just like RAM memory locations; circuit elements can be colocated with detector pixels to carry out operations, such as compression, directly. The ability to put detector, processor and memory directly on a single CMOS chip has obvious beneficial implications for size and cost. The details of this technology and some other opportunities it presents are discussed in a com-

panion JASON report, entitled “Unconventional Integration” (JSR-95-120 and JSR-95-121).

The primary issues in designing a sensor package for this application are size, cost and power consumption versus the bit rate needed to send useful video imagery. As we will see in the next subsection, the active pixel array technology seems to put all these parameters in an interesting range.

Although we have not had time to pursue the subject very far, it is clear that unconventional methods of emplacing the sensor packages will be needed (careful installation by trained technicians is obviously not a useful model). We like the idea of “fire and forget” emplacement in which the package is fired at, and sticks to, a convenient surface. The package, including the optics, would need a certain level of shock hardness and some means of ensuring that the emplaced sensor would have a useful field of view. Putting all the electronics, detection and RF elements on a single chip would confer a level of mechanical robustness which should make such emplacement schemes easier to develop.

A.2 Strawman Design of an Emplaced Video Sensor

To give a concrete sense of what can be done with the new sensor technology, we present a strawman design of a sensor/communicator package that would, supposing the optics and emplacement issues can be solved, meet the needs of our battlefield microsurveillance scheme. More details on the technology issues involved can be found in the companion JASON report entitled “Unconventional Integration”. A primary goal is to make the package as

small and light as possible. Given the communication needs, battery energy density is the primary determinant of size and weight. Zinc-air batteries, which store 20 Whr per cubic inch, are a very attractive choice: two cubic inches of battery volume give a 400 hour active lifetime at 100 mW average power consumption and correspondingly longer at lower power.

A conceptual miniature sensor based on this technology is shown in Figure A-1. The overall size is set mainly by the battery and would be 2-3 cubic inches (the proverbial pack of cigarettes). Whether this is small enough to meet the needs of the application we have in mind is not completely obvious and must be determined by further studies of quasi-realistic scenarios. Further miniaturization is possible, but, because of the communications power requirements and the realities of battery energy density, autonomous sensors with this performance are not going to be shrunk to the size of a sugar cube.

The power budget of the sensor is as follows: A 512×512 active pixel camera draws 35 mW at video rates but only 1 mW at 1 frame/s. Whether the camera is on or off, its frame rate and the level of image compression (possibly implemented directly on the sensor chip) is controlled by network input or by trigger from other sensors. A frame rate of one per second, on average, is probably higher than is really needed (though it is important to be able to go to full video on demand). Location determination by a typical GPS receiver chip draws 150 mW for about a minute. Since this has to be done only once, upon deployment, the total energy involved is negligible and the real cost is the complication of the extra GPS hardware on board the device. Non-imaging sensors will certainly be useful and could easily be included in the package. Acoustic/vibration sensors would be very useful to generate an alarm signal for explosions and weapons fire. Single sensors

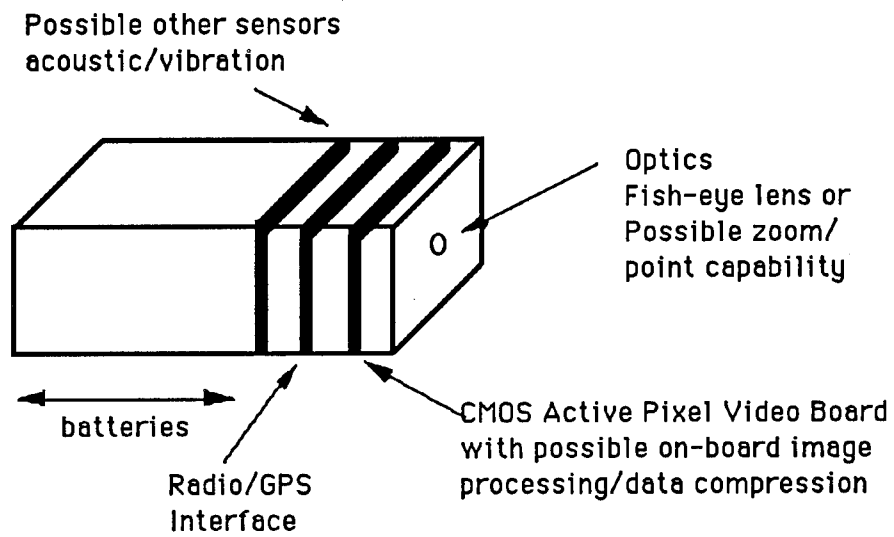


Figure A-1. Strawman layout of a miniature imaging sensor.

would probably have a large false alarm rate (from vehicle backfires and the like), but correlating the output of nearby sensors might turn this into a useful tool. At a rough guess, such sensors would draw power at a rate of 1-10mW. This would be a small component of the overall power budget.

The dominant component of the power budget is the RF power needed to transmit the data. Just to recall, with conservative assumptions about efficiencies and no antenna gain, the link powers needed for typical data rates and link ranges are (at S-band): 2 mW for 10^6 bits/s at 100m, 20 mW for 10^5 bits/s at 1000m, 200 mW for 10^4 bits/s at 10 km. Depending on how the network is configured, the required communications power should be somewhere from a few tens of mW to about 100 mW.

B APPENDIX: LOW-POWER A/D CONVERSION (This Appendix is taken from JSR-95-145, "Ultrasound")

B.1 Overview

We have already pointed out the importance of low-power analog-to-digital (A/D) conversion for large ultrasound arrays. This report analyzes the power dissipation of a straightforward A/D converter.

B.2 Block Diagram

Figure B-1 shows a block diagram of a typical A/D converter. Each sample interval an analog input signal is placed on the positive input of a comparator. The "logic" and "D/A" blocks then generates a series of voltages to which the input is compared. The output is generated as a result of these comparisons.

Different styles of A/D converters vary the sequence of voltages being compared and the manner in which they are generated. Some popular styles include:

1. Successive Approximation: The logic generates a series of voltages that perform a binary search for the input voltage by repeatedly halving the interval in which the voltage may be contained. This generates an b -bit digital output in b steps with the output of the comparator containing

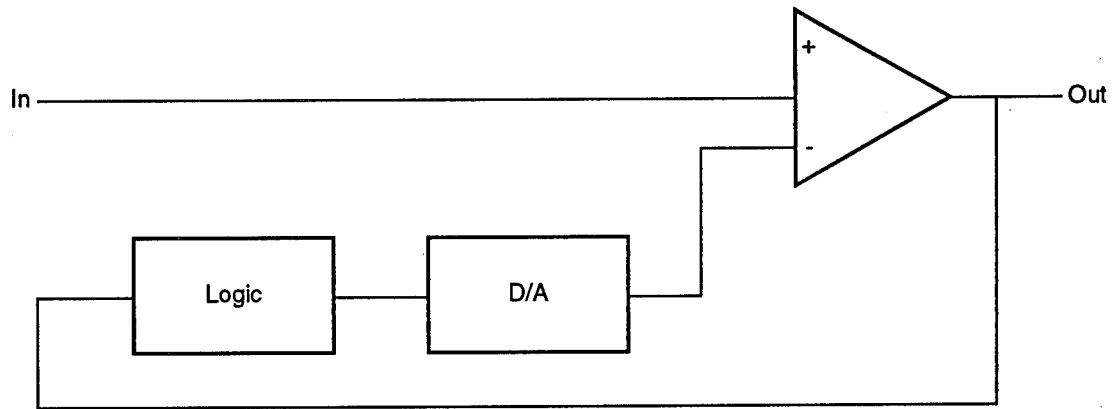


Figure B-1. A/D Converter Block Diagram.

the bits of the output MSB-first. The binary search can be performed serially in a single stage or as a pipeline of stages, one per bit.

2. Slope or Dual-Slope: The logic generates a “ramp” independent of the comparator output and the point at which the comparator switches indicates the input voltage. The ramp is usually generated by an analog integrator while the time interval is measured by sampling a free-running counter. This method requires 2^b steps to generate an b -bit output.
3. Oversampled: The logic closes a loop that “delta-codes” the input. That is the logic counts up when the output of the comparator is one and down if it is zero. Some converters use delta-sigma rather than straight delta coding. In either case an integrator can be used to generate the voltages eliminating the need for a full D/A. The output stream is decimated to produce an b -bit digital signal at 2^{-b} the original sample rate. These converters are popular in systems where the oversampling and decimation obviate the need for analog anti-aliasing filters with sharp cut-offs.
4. Flash: A flash converter performs all of the operations of a slope converter, but in parallel rather than serially. A resistive or capacitive voltage divider generates 2^b equally-spaced voltages and 2^b comparators compare the input signal to all of these voltages simultaneously. A log-depth logic circuit encodes the output of the comparators into a b -bit signal. Flash converters are used in situations where very low latency is required. For total throughput a successive approximation converter is preferred as b successive approximation converters have the same throughput as a single flash converter at $b/2^b$ the cost.

5. Hybrid: A hybrid converter is a successive approximation converter that uses an m -bit flash converter at each stage to perform a b -bit conversion in b/m steps. Rather than using a D/A in a feedback loop, the signal is usually recentered and rescaled between each step to perform the 2^m -ary divide and conquer search.

B.3 Power Calculation

Consider the problem of performing a b bit A/D conversion with sample rate f . If a successive approximation converter is used, the energy required for the conversion is

$$P_{sa} = fb(E_c + gE_{sw} + E_{sda})$$

where E_c is the energy required per comparison, E_{sw} is the switching energy of the technology, g gates switch for the logic to prepare for each comparison, and E_{sda} is the D/A conversion energy. Each of these components of power is dealt with in more detail below.

The slope-based and oversampling converters require considerably more power than this because although they have simpler logic and D/A components this advantage is overwhelmed by the fact that they perform 2^b comparisons to convert a b -bit number rather than b .

B.3.1 Comparator

The comparator can be realized as a clocked sense-amplifier, as a static

differential amplifier, or as an inverter with a switched capacitor input. In the case of the static amplifier, the current bias is set so it has just enough output current to swing its output capacitance in one bit time. A self-biasing circuit can be used to adjust the current source to this minimum current value. The output capacitance includes the self capacitance of the amplifier, a small amount of wiring capacitance, plus a minimum-sized inverter to buffer the signal for distribution to the logic. If transistor sizes are kept small a total capacitance of 50 fF is reasonable in an 0.5 μm process. Assuming half the bias current goes into the output and a 3.3V supply voltage this gives a comparison energy of

$$E_c = 5 \times 10^{-14} (3.3^2) (2) \approx 1\text{pJ}$$

With the clocked sense amplifier the clock load is increased by about 10fF to drive isolation devices and to gate on the amplifier current source. Also the regenerative feedback slightly increases the self-capacitance of the amplifier, to about 70fF for typical device sizes. Thus a clocked sense-amp would have a slightly higher comparison energy of about 1.6pJ but would have the advantage of not requiring a speed-dependent bias current.

An inverter with a switched input capacitor would have a somewhat larger power dissipation as it requires a DC current (when operated in the middle of its range), current to charge its input capacitor, and clock power to drive the switches.

B.3.2 D/A

The D/A converter can be realized using switched capacitors, with an R-2R ladder, or with a series of progressively-sized transistors. The R-2R ap-

proach will not be considered as precise-valued resistors are hard to fabricate on an MOS integrated circuit.

The switched capacitor D/A takes advantage of the subdivision property of the voltage sequence in a successive approximation A/D converter to produce the required voltage sequence by charge sharing between two equally sized capacitors. Initially one capacitor is charged high and the other low to bound the interval. A capacitive voltage divider is then used to find the midpoint of the interval. This midpoint voltage is then placed on one of the two capacitors to define the next interval and the process is repeated.

This approach requires two voltage followers that must have enough bias current to copy voltages accurately in a bit time. With 100fF capacitors, each follower would consume about 2pJ per bit and another 2pJ would be used in charging each capacitor for a total of 8pJ per bit.

The transistor approach, which to our knowledge is original, replaces the negative input of the comparator with a parallel connection of NFETs with progressively increasing sizes. Rather than being connected to an analog voltage, the gates of these transistors are directly controlled by the logic. They are sized so that the comparator will “trip” when the input voltage exceeds the binary value encoded on the transistor gates. The sizes are not simply powers of two, but rather must match the quadratic I-V characteristic of the MOSFET.

The only power consumed by this approach is caused by the increased capacitive load on the output of the logic which switches at most once per cycle. For small b , this load is small but for large b it increases exponentially.

A rough expression for the energy required per bit is:

$$E_{sda} = 0.1(2^{b/2})/bpJ$$

For an 8-bit signal, this is just 0.2pJ per bit.

Alternatively power-of-two sized transistors can be connected to a polysilicon load resistor to generate a voltage that is a linear function of the binary input. This will roughly double the comparison energy.

In either case, capacitance is minimized by using a minimum sized device in the middle of the size range and using devices with minimum L and $W > L$ in the upper half of the range and minimum W and $L > W$ in the lower half of the range.

B.3.3 Logic

The logic required for a serial successive-approximation converter is a register to hold each bit of the current digital value, and ring-counter shift register to select the next bit to update, and a MUX to select the input to each bit of the register. Each register bit toggles exactly once per conversion cycle as does each ring counter bit. If we count switching each register as four switching events and add two switching events for the associated MUX, the constant g is 10 switching events per bit. With an E_{sw} of 0.1pJ this gives a logic energy of 1pJ per bit. For a pipelined converter the ring counter and multiplexer are not required reducing this power slightly.

B.3.4 Example

For example a $b = 8$ -bit converter with a transistor D/A operating at 1 MHz would have a total power dissipation of

$$P_{sa} = 8 \times 10^6(1\text{pJ} + 0.2\text{pJ} + 1\text{pJ}) \approx 20\mu\text{W} .$$

Even if we increase this by a factor of 5 to use the 1.6pJ sense amp, the 8pJ capacitive D/A and to account for overhead the power is still only $100\mu\text{W}$.

B.4 Other Issues

B.4.1 Resolution and Linearity

To operate at very low power, one uses minimum sized devices. These devices can have relatively large parameter mismatch (on the order of 10%) which limits the linearity of the converter. It is more power efficient to correct these linearities digitally via a PROM than it is to increase the component size to eliminate them.

To get adequate resolution in the presence of mismatches, capacitor leakage, and other effects, the converter may have to produce more bits of intermediate result than are required in the final linearized result. The converter must resolve voltage steps that are no more than one LSB apart. Usually adding one additional bit is sufficient to provide this spacing.

B.4.2 Low-Voltage Operation

The analysis above has not considered the possibility of voltage scaling. If the circuit is operated slowly, the supply voltage can be reduced which reduces power quadratically. While very slow circuits can be operated in the subthreshold region, most practical circuits are limited to supply voltages of about 1V to remain comfortably above the device threshold. At 1V power is reduced by a factor of 9 over the numbers calculated above. Low voltage operation does require that the input voltage be scaled to the small power supply.

C APPENDIX: AEROSOL GENERATORS

It is sometimes necessary to make large numbers of very small (radii $\sim 1\mu$) drops of liquid. If water is forced through a small nozzle it breaks up into droplets. This is called hydraulic atomization, and a phenomenological expression for the mean droplet radius is given in the *McGraw-Hill Encyclopedia of Science and Technology*:

$$r = \frac{1}{2} \frac{5d}{N_{\text{Re}}^{0.15} N_{\text{We}}^{0.20}}, \quad (\text{C-1})$$

where d is the nozzle diameter, $N_{\text{Re}} \equiv \frac{du\rho}{\mu}$ is the Reynolds number, $N_{\text{We}} \equiv \frac{du^2\rho}{\sigma}$ is the Weber number, u is the fluid velocity, ρ is its density, μ is its dynamic viscosity and σ is its surface tension. It is clear that to produce small droplets requires small nozzles and high fluid speeds. The fluid speed may be related to the pressure drop p by Bernoulli's equation $\frac{u^2}{2} = \frac{p}{\rho}$, assuming the entire pressure drop occurs across the nozzle. Small nozzles are made for ink jet printers by anisotropic etching of silicon (E. Bassous, H. H. Taub and L. Kuhn *Appl. Phys. Lett.* **31**, 135, 1977), and this mature technology can be used. Figure C-1 shows a portion of the suggested array of nozzles. The angle of the silicon nozzles is determined by its properties of anisotropic etch; the wedge shown has an angle of $54.7^\circ = \tan^{-1} \sqrt{2}$. The nozzles are square pyramidal frusta, with each side of the square aperture taken to be 10μ , which is used for the nozzle diameter d in the expression for the droplet size. The bases of the pyramidal frusta are squares whose sides are 150μ . The nozzles are spaced, center-to-center, at distances of 250μ in a square array on a wafer 100μ thick.

The direction of flow is taken to be opposite to that used in ink jet printers. In an ink jet printer the nozzles are full of fluid, which pushes

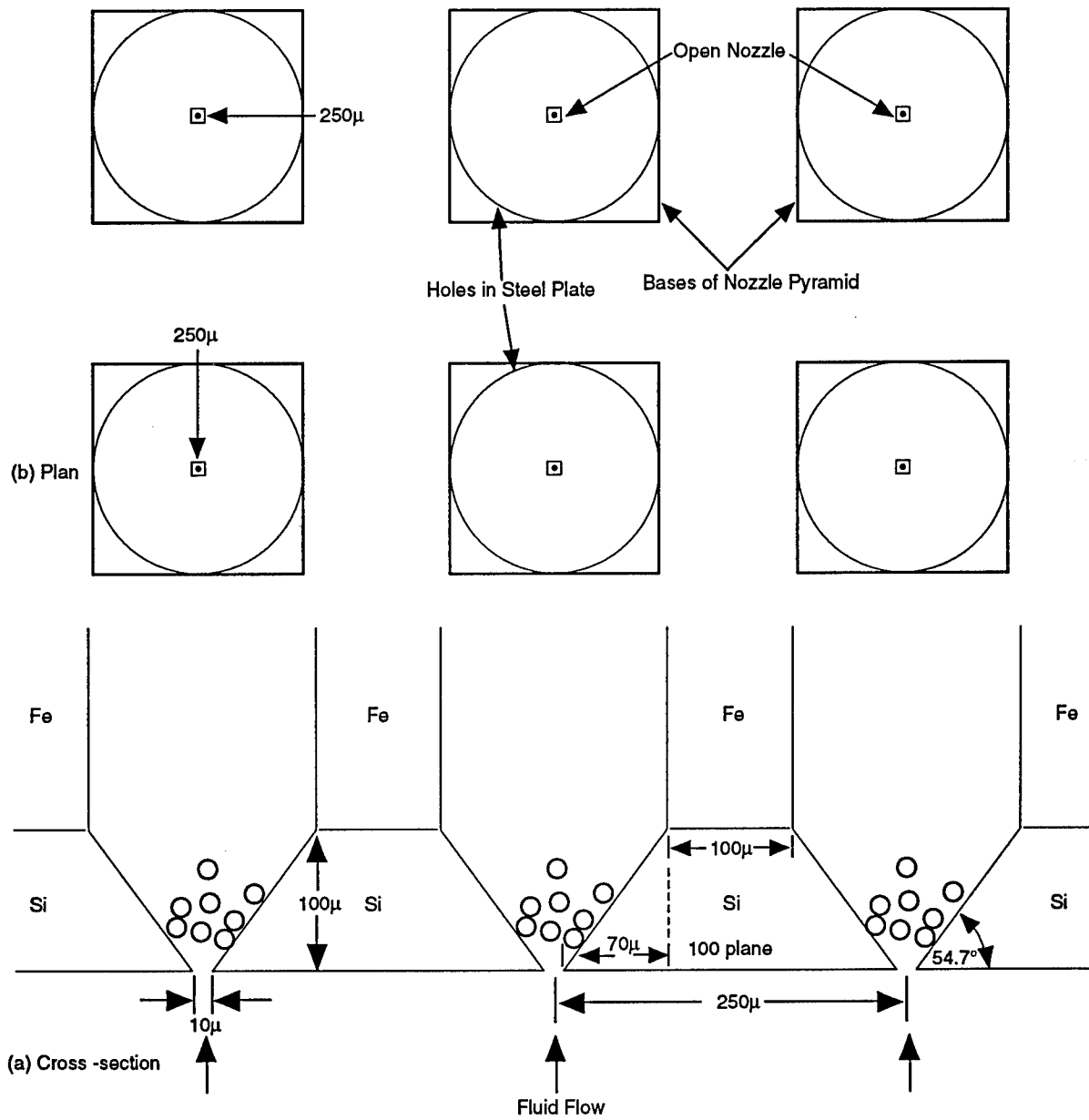


Figure C-1. Nozzle design, including supporting steel, etched anisotropically in 100 Si water, 100µ thick. Nozzles are on 250µ centers.

outward on the walls of the nozzle. The stress is largely tensile, and its concentration at these sharp edges would threaten the brittle silicon with catastrophic failure. This is not a danger in the printer, in which the ink is at low pressure, but would be a serious problem at the high pressures required in the atomizer. With the indicated direction of flow the nozzles contain only air at atmospheric pressure and tiny droplets of liquid which do not contact its walls, so there is no tensile stress to concentrate. We assume $p = 100$ bars = 1500 psi, within the range of hydraulic technology (pressures up to 5000 psi are used). Then Bernoulli's equation implies a fluid discharge velocity $u = 1.4 \times 10^4$ cm/sec, $N_{Re} = 1400$ and $N_{We} = 3000$. The mean drop radius is then $r \approx 1.7 \mu$. The total mass of solution required to make 10^{17} drops is 2 tons, which can be carried on an aircraft of moderate size, or atomized on the ground. Smaller nozzles would produce smaller droplets, with $r \propto d^{0.65}$. The total mass flow rate through the nozzle is proportional to its area d^2 , and the mass of each droplet is $\propto r^3 \propto d^{1.95}$. Hence the number of droplets produced per unit time, which is the important parameter, is essentially independent of the nozzle dimensions and is

$$\dot{N} \approx 7 \times 10^8 \left(\frac{p}{1500 \text{ psi}} \right)^{1.33} \text{ sec}^{-1}. \quad (\text{C-2})$$

Nozzles even smaller than 10μ are therefore desirable, if they can be made, because they consume less fluid. We assume $d = 10 \mu$ only because it appears to be readily manufacturable with standard silicon technology, without extraordinary control on the wafer thickness and uniformity of the etch rate.

Fluid flows through each nozzle at a rate $ud^2 = 1.4 \times 10^{-2}$ cm³/sec, or 50 cm³/hr. In order to atomize the entire 2 tons of solution (into 10^{17} drops) in an hour would require 40,000 nozzles. The hydraulic power required is about 6 kW, which is feasible. The nozzle array may be fabricated from a single silicon wafer at 250μ spacing in an array 5 cm square. However, such

a single large array would be vulnerable to breakage. We therefore consider 100 separate silicon chips, each containing 400 nozzles filling an area of 0.25 cm². Each chip would be circular, with diameter of about 6 mm, and each would be mounted at the end of a pipe containing the pressurized solution. The silicon chips separate a region of pressurized liquid at 1500 psi from air at atmospheric pressure. A chip 100 μ thick and 6 mm in diameter cannot hold such a pressure drop. A thicker slab of silicon would be stiffer, but because the angle of anisotropic etch is fixed the width of the bases of the nozzles increases in proportion to the slab's thickness, as does their spacing. The diameter of a chip containing a given number of nozzles must therefore also increase in proportion to its thickness. The peak stress is then independent of thickness and depends only on (and is proportional to) the number of individual nozzles. Silicon can tolerate a tensile stress of roughly 15,000 psi, so that if silicon alone is used each chip could contain only a few nozzles, and many thousand chips would be required, each with its own plumbing.

We suggest instead that the silicon chips be backed with a perforated steel plate, as shown in Figure C-1. The steel would contain holes 150 μ (6 mils) in diameter aligned with the nozzles in the silicon. Holes of this size can be drilled by electric discharge machining. A single 400 wire tool could drill the required steel plate in a single operation. The required thickness of a uniform plate is determined by the maximum tolerable stress S_m (*Standard Handbook for Mechanical Engineers*) as

$$h = \left(\frac{kpr^2}{S_m} \right)^{1/2}, \quad (C-3)$$

where the constant k is 1.24 for simply supported edges and 0.75 for fixed edges. The perforated plate we discuss has 30% of its volume drilled out, whose effect we approximate by dividing these values of k by 0.7. Adopting $S_m = 3$ Kbar as a safe stress for steel and $k = 1.8$ for simply supported edges

yields $h = 0.24r$, or $h = 0.72$ mm for a 6 mm diameter disc. This is a modest thickness, and implies holes only five times as long as their diameters, so that few droplets should be lost by contacting the sides of the holes. For comparison, the stress in a silicon chip unsupported by steel would be over 100 Kbar, far above its strength. Some droplets will inevitably strike the sides of the holes in the steel, raising the concern that if enough solution sticks to them the holes will fill with liquid and clog. It is uncertain that this is actually a danger, because high velocity impact will tend to splash wetting fluid off the surface and out the open end of the hole. Applying a hydrophobic film to the steel would also reduce the danger of clogging; small holes in a hydrophobic material are difficult to wet, even without the cleansing action of the stream of droplets.

The silicon is pressed against the steel plate by the pressure of the fluid. With negligible stiffness of its own because of its thinness, it acts as a compliant membrane, and assumes the shape of the steel. The Young's moduli of steel (1.9–2.1 Mbar) and silicon (1.9 Mbar) are very similar, so the stress, as well as the strain, in the silicon are nearly the same as in the steel against which it is pressed. The maximum tolerable tensile stress for silicon is about 1 Kbar. Here the tolerable mean tensile stress may be much less because of stress concentration at the edges of the pyramidal nozzles. However, because the silicon is on the concave side of the bent steel plate (concavity across the plate is assured by the use of simply supported edges) it is everywhere in compression; brittle substances are generally able to tolerate compressive loads substantially in excess to their strength in tension. If, even so, the stress on the silicon is too high it may be reduced by thickening the steel plate or by adding stiffening ribs to it; for example, increasing h to 1.25 mm reduces all stresses below 1 Kbar.

References

- [1] Analog Devices, Monolithic Accelerometer ADXL50 Data Sheet T. B. Gabrielson, "Mechanical-Thermal Noise in Micromachined Acoustic and Vibration Sensors", IEEE Transactions on Electron. Devices, 40, 903, 1993.
- [2] C. Mead, "A sensitive electronic photoreceptor," 1985 Chapel Hill Conference on VLSI, pp. 463-471, 1985.
- [3] E.R. Fossum, "Ultra-low power imaging systems using CMOS image sensor Technology," Proceedings of the SPIE, vol 2267, Advanced Microdevices and Space Science Sensors (1994).
- [4] A. Flynn, "Piezoelectric Ultrasonic Micromotors", Doctoral Dissertation, MIT, 1995.
- [5] A. M. Flynn, et al. "Piezo-electric Micromotors for Microrobots," J. Micro electromechanical Systems 1, 44 (1992).
- [6] K.R. Udayakumar, et al., "Ferroelectric Thin Film Ultrasonic Micromotors," Ferroelectrics, 160, 347, 1995.
- [7] D. Haronian and N.C. MacDonald, "A Microelectromechanics Based Artificial Cochlea", to be published, 1995.
- [8] J. J. Yao, S. Arney, and N. MacDonald, "A fully suspended, movable, single-crystal silicon, deep submicron MOSFET for nanoelectromechanical applications," Sensors and Actuators A40, 77, 1994.
- [9] W.J. Kaiser, "New high-sensitivity microaccelerometer technology for vibration control," preprint, 1995.

- [10] T.W. Kenny, et al. "Wide-Bandwidth Electromechanical Actuators for Tunneling Displacement Transducers," *J. Microelectromechanical Systems* 3, 9, 1994.
- [11] E.A. Dobisz and C.R. K. Marrian, "Scanning tunneling microscope lithography: A solution to electron scattering," *J. Vac. Sci. Technol. B9*, 3024 1991
- [12] P.M. Campbell, E.S. Snow and P.J. McMarr, "Fabrication of nanometer-scale side-gated silicon field effect transistors with an atomic force microscope," *Appl. Phys. Lett.* 66, 1388 1995.
- [13] S.C. Minne, H.T. SOh, Ph. Flueckiger, and C.F. Quate, "Fabrication of 0.1 μm metal oxide semiconductor field effect transistors with the atomic force microscope," *Appl. Phys. Lett.* 66, 703, 1995.
- [14] H. Ryssel, et. "Ion Beam Exposure of Resists," *Appl Phys A* 27, 239 (1982).
- [15] S.W. Park, H.T. Soh, C.F. Quate, and S.-I. Park, "Nanometer Scale Lithography at High Scanning Speeds with the Atomic Force Microscope Using Spin-On-Glass," submitted to *Appl. Phys. Lett.*, May 1995.
- [16] J.J. Mamin and D. Rugar, "Thermomechanical writing with an atomic force microscope tip," *Appl. Phys. Lett.* 61, 1003, 1992.
- [17] Y. Xu, S. Miller, and N.C. MacDonald, "Microelectromechanical Scanning Tunneling Microscope," to be published, 1995.
- [18] S.C. Minne, Ph. Flueckiger, H.T. Soh, and C.F. Quate, "Atomic force microscope lithography using amorphous silicon as a resist and advances in parallel operation," *J. Vac. Sci. Technol B13*, 1380, 1995.

- [19] M. Prentiss, G. Timp and N. Bigelow, "Using light as a stencil", Appl Phys Lett., Vol 60, **1027** (1992).
- [20] R. Gupta, J. J. McClelland and R. J. Celotta, "Nanofabrication of a two-dimensional array using laser-focused atomic deposition", Appl. Phys. Lett., Vol 67, **1278** (1995).

DISTRIBUTION LIST

Director of Space and SDI Programs
SAF/AQSC
1060 Air Force Pentagon
Washington, DC 20330-1060

CMDR & Program Executive Officer
U S Army/CSSD-ZA
Strategic Defense Command
PO Box 15280
Arlington, VA 22215-0150

A R P A Library
3701 North Fairfax Drive
Arlington, VA 22209-2308

Dr Arthur E Bisson
Director
Technology Directorate
Office of Naval Research
Room 407
800 N. Quincy Street
Arlington, VA 20350-1000

Dr Albert Brandenstein
Chief Scientist
Office of Nat'l Drug Control Policy
Executive Office of the President
Washington, DC 20500

Mr. Edward Brown
Assistant Director
ARPA/SISTO
3701 North Fairfax Drive
Arlington, VA 22203

Dr H Lee Buchanan, I I I
Director
ARPA/DSO
3701 North Fairfax Drive
Arlington, VA 22203-1714

Dr Ashton B Carter
Nuclear Security & Counter Proliferation
Office of the Secretary of Defense
The Pentagon, Room 4E821
Washington, DC 20301-2600

Dr Collier
Chief Scientist
U S Army Strategic Defense Command
PO Box 15280
Arlington, VA 22215-0280

Dr Ken Cress
Office of Research and Development
Washington, DC 20505

DTIC [2]
Cameron Station
Alexandria, VA 22314

Dr William Dally
University of North Carolina
Department of Computer Science
Sitterson Hall, Campus Box 3175
Chapel Hill, NC 27599

Mr John Darrah
Senior Scientist and Technical Advisor
HQAF SPACOM/CN
Peterson AFB, CO 80914-5001

Dr Victor Demarines, Jr.
President and Chief Exec Officer
The MITRE Corporation
202 Burlington Road
A210
Bedford, MA 01730-1420

Dr Alvin Despain
3273 Corinth Avenue
Los Angeles, CA 90066

Dr Douglas Eardley
618 Miramonte Drive
Santa Barbara, CA 93109

DISTRIBUTION LIST

Mr Dan Flynn [5]
OSWR
Washington, DC 20505

Dr Paris Genalis
Deputy Director
OUSD(A&T)/S&TS/NW
The Pentagon, Room 3D1048
Washington, DC 20301

Dr Lawrence K. Gershwin
NIC/NIO/S&T
7E47, OHB
Washington, DC 20505

Dr David Hammer
109 Orchard Place
Ithaca, NY 14850

Mr. Thomas H Handel
Office of Naval Intelligence
The Pentagon, Room 5D660
Washington, DC 20350-2000

Dr Robert G Henderson
Director
JASON Program Office
The MITRE Corporation
7525 Colshire Drive
Mailstop Z561
McLean, VA 22102

Dr Paul Horowitz
Harvard University
Lyman Laboratory of Physics
Cambridge, MA 02138

Dr William E Howard III [2]
Director of Advanced Concepts &
Systems Design
The Pentagon Room 3E480
Washington, DC 20301-0103

Dr Gerald J Iafrate
U S Army Research Office
PO Box 12211
4330 South Miami Boulevard
Research Triangle NC 27709-2211

J A S O N Library [5]
The MITRE Corporation
Mail Stop W002
7525 Colshire Drive
McLean, VA 22102

Dr Anita Jones
Department of Defense
DOD, DDR&E
The Pentagon, Room 3E1014
Washington, DC 20301

Mr. O' Dean P. Judd
Los Alamos National Laboratory
Mailstop F650
Los Alamos, NM 87545

Dr Bobby R Junker
Office of Naval Research
Code 111
800 North Quincy Street
Arlington, VA 22217

Dr Jonathan Katz
Washington University
Department of Physics
St Louis, MO 6333130

Lt Gen, Howard W. Leaf, (Retired)
Director, Test and Evaluation
HQ USAF/TE
1650 Air Force Pentagon
Washington, DC 20330-1650

Dr Nathan Lewis
California Institute of Technology
Division of Chemistry and
Chemical Engineering: 127-72
Pasadena, CA 91125

DISTRIBUTION LIST

Mr. Larry Lynn
Director
ARPA/DIRO
3701 North Fairfax Drive
Arlington, VA 22203-1714

Dr. John Lyons
Director of Corporate Laboratory
US Army Laboratory Command
2800 Powder Mill Road
Adelphi, MD 20783-1145

Col Ed Mahen
ARPA/DIRO
3701 North Fairfax Drive
Arlington, VA 22203-1714

Dr. Arthur Manfredi
OSWR
Washington, DC 20505

Mr James J Mattice
Deputy Asst Secretary
(Research & Engineering)
SAF/AQ
Pentagon, Room 4D-977
Washington, DC 20330-1000

Dr George Mayer
Office of Director of Defense
Reserach and Engineering
Pentagon, Room 3D375
Washington, DC 20301-3030

Dr Bill Murphy
ORD
Washington, DC 20505

Mr Ronald Murphy
ARPA/ASTO
3701 North Fairfax Drive
Arlington, VA 22203-1714

Dr Julian C Nall
Institute for Defense Analyses
1801 North Beauregard Street
Alexandria, VA 22311

Dr. Wolfgang K. Panofsky
Stanford Linear Accelerator Center
Stanford University
P. O. Box 4349
Stanford, CA 94039

Dr Ari Patrinos
Director
Environmental Sciences Division
ER74/GTN
US Department of Energy
Washington, DC 20585

Dr Bruce Pierce
USD(A)D S
The Pentagon, Room 3D136
Washington, DC 20301-3090

Mr John Rausch [2]
Division Head 06 Department
NAVOPINTCEN
4301 Suitland Road
Washington, DC 20390

Records Resource
The MITRE Corporation
Mailstop W115
7525 Colshire Drive
McLean, VA 22102

Dr Victor H Reis
US Department of Energy
DP-1, Room 4A019
1000 Independence Ave, SW
Washington, DC 20585

Dr Fred E Saalfeld
Director
Office of Naval Research
800 North Quincy Street
Arlington, VA 22217-5000

DISTRIBUTION LIST

Dr Dan Schuresko
O/DDS&T
Washington, DC 20505

Dr John Schuster
Technical Director of Submarine
and SSBN Security Program
Department of the Navy OP-02T
The Pentagon Room 4D534
Washington, DC 20350-2000

Dr Michael A Stroschio
US Army Research Office
P. O. Box 12211
Research Triangle NC 27709-2211

Dr Jeremiah Sullivan
604 Burkwood Ct. E.
Urbana, IL 61801

Superintendent
Code 1424
Attn Documents Librarian
Naval Postgraduate School
Monterey, CA 93943

Ambassador James Sweeney
Chief Science Advisor
USACDA
320 21st Street NW
Washington, DC 20451

Dr George W Ullrich [3]
Deputy Director
Defense Nuclear Agency
6801 Telegraph Road
Alexandria, VA 22310

Dr Walter N Warnick [25]
Deputy Director
Office of Planning & Analysis, ER-5.1
Office of Energy Research
U S Department of Energy
Germantown, MD 2074

Dr Robert Westervelt
Harvard University
Division of Applied Sciences
Cambridge, MA 02138

Dr Edward C Whitman
Dep Assistant Secretary of the Navy
C3I Electronic Warfare & Space
Department of the Navy
The Pentagon 4D745
Washington, DC 20350-5000

Capt H. A. Williams, U S N
Director Undersea Warfare Space
& Naval Warfare Sys Cmd
PD80
2451 Crystal Drive
Arlington, VA 22245-5200